Electronic Supplementary Material (ESI) for ChemComm.

Unusually Short Unsupported Au(III)···Au(III) Aurophilic Contacts in Emissive Lanthanide Tetracyanoaurate(III) Complexes

Thomas E. Karpiuk, Samyadeb Mahato, Tim Storr and Daniel B. Leznoff*

Department of Chemistry, Simon Fraser University, 8888 University Drive, Burnaby, British Columbia, V5A 1S6, Canada. E-mail: dleznoff@sfu.ca

Experimental Section

General Procedures and Materials

All materials were obtained from commercial sources and used as received. IR spectra were collected using a Thermo Nicolet Nexus 670 FTIR spectrometer equipped with a Pike MIRacle ATR sampling accessory (Ge crystal; 4000–700 cm^{-1}). A Renishaw inVia Raman microscope equipped with a 514 nm laser was used to collect Raman spectra (3200–100 cm^{-1}). Microanalyses (C, H, N) were performed by Yaghoub Alkhansa at Simon Fraser University on a Thermo Fisher Scientific Flash*Smart* CHNS elemental analyzer.

Synthesis of 1Ln (Ln = Lu, Tb, Eu, Ce)

0.05 mmol (18–19 mg) of the appropriate $LnCl_3 \cdot xH_2O$ salt (x = 7, Ce; x = 6, Eu, Tb, Lu) was dissolved with 2,2'-bipyridine-*N*,*N*'-dioxide (38 mg, 0.2 mmol) in 2 mL of water. A solution of $KAu(CN)_4$ (51 mg, 0.15 mmol) in 2 mL of water was then added to the first solution dropwise. Any immediate precipitate that formed was redissolved with mild heating and stirring. Allowing the solution to slowly evaporate afforded crystals of $[Ln(bipyO_2)_4][Au(CN)_4]_3 \cdot H_2O$ (**1Ln**) after 2–4 days, which were filtered and washed with water. Yields and observations, IR and Raman data, and elemental analyses for the **1Ln** (Ln = Lu, Tb, Eu, Ce) compounds are included below (Tables S6–S9). A picture displaying a large single crystal of **1Ce** is also included as Figure S11.

Photoluminescence Spectroscopy Analysis

Solid-state photoluminescence spectra were collected using an Edinburgh Instruments FS5 spectrofluorometer equipped with a 150W xenon arc lamp, using samples ground to a fine powder. For measurements at 77 K, samples were loaded into an NMR tube and then submerged in liquid nitrogen using a Photon Technology International Cold Finder Dewar accessory. Commission internationale de l'éclairage (CIE) chromaticity coordinates were calculated from the emission spectra using the Edinburgh Instruments Fluoracle® software.

Quantum yield measurements were conducted also with the Edinburgh Instruments FS5 spectrofluorometer. The methods described by Morse et al.[1] and da Silva et al.[2] were adapted, using sodium salicylate as a reference standard. KBr was ground to a fine powder then distributed into a sample cup and the surface smoothed. An emission spectrum was collected from 20 nm below the excitation wavelength through to 750 nm, providing a spectrum showing the reflected excitation light as well as the background through the expected emission region. The analyte (either standard or sample) was then diluted appropriately with KBr and ground to a fine powder, then measured in the same way. With the analyte in the excitation path the reflected excitation light is diminished; this difference corresponds to the number of photons absorbed by the sample. The number of emitted photons can be determined from the sample emission peaks after subtracting the background. In each case, this process was repeated 3–4 times with successive KBr dilution. The quantum yield can thus be conveniently derived from the least squares linear fit of a plot of photons emitted versus photons absorbed (with y-intercept constrained to be zero).

The measured quantum yields were calibrated with respect to the reference standard sodium salicylate, which has a reported quantum yield of 60%.[3] The quantum yield measured by us was found to be 65(3)% with an excitation wavelength of 340 nm and so a correction factor of 0.92(4) was applied to the quantum yields measured for each sample. This method of acquiring quantum yield values is generally accepted to be accurate to within ±10% (relative error).[2]

X-Ray Crystallographic Analysis

Single-crystal structures were collected using a Bruker SMART diffractometer equipped with a Bruker PHOTON II 14 CPAD detector and a TRIUMPH monochromated Mo K_α (λ = 0.71073 Å) sealed tube X-Ray source. Samples were mounted using parabar oil and MiTeGen Micromounts, then cooled to 100 K using an Oxford Cryosystems Cryostream 700. Experiments were conducting using ϕ and ω scans. Diffraction data was processed using the Bruker APEX4 software suite, using the program SADABS or TWINABS; multi-scan absorption corrections and additional spherical absorption corrections using the measured crystal dimensions and calculated absorption coefficients were employed.[4] Structures were solved using the SHELXT intrinsic phasing method.[5] Structures were refined using OLEX2[6] with the SHELXL least-squares refinement algorithm.[7] Diagrams were prepared using VESTA[8] with 50% probability displacement ellipsoids or with Mercury[9] (Figure S2).

The **1Lu** crystal was found to have non-merohedral twinning, with the second domain related by a 180° rotation around the [100] direction in real space. The twinned data was processed using the programs CELL_NOW and TWINABS, structure solution was conducted using the detwinned and merged data, while final refinement was conducted using the domain-separated reflection data.[10] An additional interstitial water O10 could be located within the structure and its occupancy was allowed to refine freely, resolving to 0.329(15). In the **1Tb**, **1Eu**, and **1Ce** structures, the O10 occupancy was found to refine to 0.172(11), 0.253(12), and 0.199(8),

respectively. Based on the crystallographic and microanalysis results, this water molecule can be assumed to easily dehydrate over time and is not included in the molecular formulas. No twinning was observed with the **1Tb**, **1Eu**, and **1Ce** structures. Crystallographic data for **1Lu**, **1Tb**, **1Eu**, and **1Ce** is included below in Table S10 and is also available from the Cambridge Crystallographic Data Centre as CCDC 2324492–2324495. The crystal structure of **1Eu** was also collected and redetermined at 300 K and confirmed to be isomorphous (Orthorhombic *Pbca* with a = 20.4359(18) Å, b = 24.030(2) Å, c = 24.079(2) Å).

The powder X-Ray diffraction pattern of **1Eu** was collected using a ground sample of single-crystalline **1Eu**, mounted on the Bruker SMART diffractometer as described above. A Cu K_α (λ = 1.54184 Å) IμS microfocus X-Ray source equipped with HELIOS multi-layer optics was used for the experiment. Data was collected at 300 K with a detector distance of 150 mm, using a spinning ϕ scan (120° min^{-1}). Data was processed using the Bruker APEX IV software suite and Mercury[14] was used to simulate powder patterns from single-crystal data. The powder X-Ray diffraction pattern of **1Eu** alongside simulated data is included in Figure S12.

Computational Details

Calculations were conducted using the Gaussian 16 program (Revision A.03)[11] at the MP2 level using the def2TZVP basis set,[12–14] and the Douglas-Kroll-Hess 2nd order scalar relativistic correcton.[15] Single point calculations in the gas phase were performed using the **1Lu** initial crystal structure geometry with all molecules removed (including the $[Lu(bipyO_2)_4]^{3+}$ cation) except two $[Au(CN)_4]^-$ units (Au1 and Au2). Varying the Au···Au distance between the two $[Au(CN)_4]^-$ units provided an energy minima at *ca.* 3.5 Å, as shown in Figure S6.

Methods for SHAPE Analysis

SHAPE analysis was conducted using the SHAPE Version 2.1 software,[16–18] using atomic coordinates derived from the crystal structure geometries. Continuous shape measures quantify the percent deviation of a structure from an ideal geometry. In this case, the $[Ln(bipyO_2)_4]^{3+}$ $[LnO_8]$ coordination spheres are compared to reference polyhedra representing the common eight-coordination coordination geometries (cubic, square antiprismatic, dodecahedral, and bicapped trigonal prismatic). Shape measures of $[Ln(bipyO_2)_4]^{3+}$ complexes are included in Table S3. Minimum distortion path analysis was also conducted, where the percent deviation of the $[LnO_8]$ shape from an interconversion path between two reference polyhedral can be calculated; given that the shape lies along the interconversion path, the position along the path can also be determined (where 0% and 100% represent the shapes of the two end members, respectively). Minimum distortion path results are shown in Table S4. For visualization of the complexes' shapes, the continuous shape measures of selected $[Ln(bipyO_2)_4]^{3+}$ complexes have been plotted on the square antiprismatic-cubic shape map alongside selected ideal polyhedral, as shown in Figure S3.

Supplementary Tables

Table S1 Summary of reported unsupported Au(III) interactions.*

Compound	Distance (Å)	Type	Ref
$[AuCl_2(dpa)][AuCl_4]$	3.7467(1)	Cation-cation	[19]
$[Au(TBPP)]_2[AuCl_4][AuCl_2]\cdot 2HOAc$	3.718	Cation-anion	[20]
$[AuCl_2(bpm)][AuCl_4]$	3.6540(3), 3.8701(3)	Cation-anion	[19]
$[Au(MeC\text{^}N\text{^}N)(L_1)](PF_6)$	3.6018	Cation-cation	[21]
$Au(TBPP)[AuCl_4]$	3.566	Cation-anion	[20]
$[AuBr_2(bipy)][AuBr_4]$	*ca.* 3.54†	Cation-anion	[22]
$[AuCl_2(bipy)][AuCl_4]$	3.5250(1)	Cation-anion	[19]
$[AuCl_2(bipy)][AuBr_4]$	3.518(1)	Cation-anion	[22]
$(Me_4N)[Au(N)_3]$	3.507(3), 3.584(3)	Anion-anion	[23]
$[AuBr_2(bpm)][AuBr_4]$	3.5047(1)	Cation-anion	[19]
$[Au(C\text{^}N\text{^}N)(L_2)](PF_6)$	3.495	Cation-cation	[24]
$[Lu(bipyO_2)_4][Au(CN)_4]_3\cdot 1.33H_2O$	3.3603(4), 3.4354(4)	Anion-anion	This Work

*Where dpa = 2,2'-dipyridylamine, $TBPPH_2$ = 5,10,15,20-tetrakis(4-butoxyphenyl)porphyrin, bpm = 2,2'-bipyrimidine, MeHC^N^N = 6-(4-tolyl)-2,2'-bipyridine, HL_1 = 4-ethylphenylacetylene, bipy = 2,2'-bipyridine, HC^N^N = 6-phenyl-2,2'-bipyridine, HL_2 = 4-(*N*,*N*'-dimethylamino)-phenylacetylene, $bipyO_2$ = *N*,*N*'-dioxide-2,2'-bipyridine. †Poor quality crystallographic data.

Table S2 Measured Inter-ligand Centroid-centroid Distances of $[Ln(bipyO_2)_4]^{3+}$ Complexes[3,25,26]*

	Centroid-centroid 1	Centroid-centroid 2
1Lu	6.046	5.876
1Tb	6.070	5.884
1Eu	6.081	5.885
1Ce	6.116	5.891
$Lu(bipyO_2)_4(ClO_4)_3\cdot 2H_2O$	3.695	3.665
$Nd(bipyO_2)_4(ClO_4)_3$	3.805	3.739
$La(bipyO_2)_4(ClO_4)_3$	3.758	3.621

*See Figure S1 (below) for example of centroid-centroid distances.

Table S3 Continuous Shape Measures (%) of $[Ln(bipyO_2)_4]^{3+}$ Complexes[3,25,26]*

	Cubic (O_h)	SAP (D_{4d})	Dod (D_{2d})	BTP (C_{2v})
1Lu	9.588	2.093	**0.308**	2.139
1Tb	9.342	2.107	**0.301**	2.155
1Eu	9.299	2.072	**0.312**	2.137
1Ce	8.992	2.055	**0.368**	2.193
$Lu(bipyO_2)_4(ClO_4)_3 \cdot 2H_2O$	5.283	1.435	**1.256**	2.928
$Eu(bipyO_2)_4(ClO_4)_3$†	3.293, 2.699	2.708, 3.442	**2.364, 2.677**	4.329, 5.093
$Nd(bipyO_2)_4(ClO_4)_3$	2.873	3.101	**2.424**	4.721
$La(bipyO_2)_4(ClO_4)_3$	**0.171**	8.899	6.503	10.836

*Smallest deviation for each compound shown in **bold**. Where SAP = square antiprismatic, Dod = dodecahedral, and BTP = bicapped trigonal prismatic. †The two values correspond to the geometries of the crystallographically distinct Eu1 and Eu2 atoms, respectively, reported in the published structure of $Eu(bipyO_2)_4(ClO_4)_3$.

Table S4 Minimum Distortion Paths (%) of Selected $[Ln(bipyO_2)_4]^{3+}$ Complexes[3,25]*

	0%	100%	Path Deviation	Path Position
$Lu(bipyO_2)_4(ClO_4)_3 \cdot 2H_2O$	Cubic (O_h)	SAP (D_{4d})	**4.2**	**68.6**
	SAP (D_{4d})	Dod (D_{2d})	37.0	N/A
	Cubic (O_h)	Dod (D_{2d})	20.4	N/A
$Eu(bipyO_2)_4(ClO_4)_3$†	Cubic (O_h)	SAP (D_{4d})	**2.9, 4.1**	**54.0, 48.8**
	SAP (D_{4d})	Dod (D_{2d})	88.5, 107	N/A
	Cubic (O_h)	Dod (D_{2d})	17.8, 15.2	N/A
$Nd(bipyO_2)_4(ClO_4)_3$	Cubic (O_h)	SAP (D_{4d})	**2.8**	**50.4**
	SAP (D_{4d})	Dod (D_{2d})	96.6	N/A
	Cubic (O_h)	Dod (D_{2d})	14.3	N/A

*Smallest path deviations for each compound shown in **bold**, alongside corresponding path positions. Path positions not shown in cases where the path deviation is greater than 10%. Where SAP = square antiprismatic, Dod = dodecahedral, and BTP = bicapped trigonal prismatic. †The two values correspond to the geometries of the crystallographically distinct Eu1 and Eu2 atoms, respectively, reported in the published structure of $Eu(bipyO_2)_4(ClO_4)_3$.

Table S5 Selected Bond Lengths (Å) for **1Lu***

Au1···Au2	3.3603(4)
Au2···Au3	3.4354(4)
Au1···N1	3.040(6)
O1···N1	3.111(16)
O1···N2	3.002(16)
O2···N3	3.157(9)

*See Figure S3 (below) for reference.

Table S6 Yields and Observations for **1Ln**

Lanthanide	**Yield**		**Observations**
	(mg)	(%)	
Lu	41	44	Colourless plate-like crystals
Tb	43	47	Colourless plate-like crystals that emitted bright-green light under broadband ultraviolet (UV) light irradiation
Eu	19	21	Colourless plate-like crystals that emitted bright-red light under broadband UV light irradiation
Ce	40	44	Large plate-like orange crystals

Table S7 IR data for **1Ln**

Lanthanide	**Frequency** (ATR, cm^{-1})
Lu	3099 (ν_{OH}, w), 1620 (δ_{OH}, vw), 1478 (m), 1449 (w), 1431 (m), 1429 (m), 1260 (ν_{NO}, m), 1245 (ν_{NO}, s), 1235 (ν_{NO}, m), 1218 (ν_{NO}, s), 1160 (vw), 1125 (vw), 1106 (vw), 1034 (vw), 852.7 (m), 838.7 (m), 773.1 (m), 765.8 (m), 722.3 (vw)
Tb	3092 (ν_{OH}, w), 1619 (δ_{OH}, vw), 1478 (m), 1446 (w), 1431 (m), 1429 (m), 1259 (ν_{NO}, m), 1242 (ν_{NO}, s), 1233 (ν_{NO}, m), 1217 (ν_{NO}, s), 1160 (vw), 1125 (vw), 1107 (vw), 1035 (vw), 852.6 (m), 837.5 (m), 772.9 (m), 765.4 (m), 723.2 (m)
Eu	3100 (ν_{OH}, w), 1619 (δ_{OH}, vw), 1478 (m), 1446 (w), 1431 (m), 1429 (m), 1260 (ν_{NO}, m), 1241 (ν_{NO}, s), 1232 (ν_{NO}, m), 1217 (ν_{NO}, s), 1160 (vw), 1124 (vw), 1106 (vw), 1036 (vw), 852.5 (m), 836.5 (m), 772.7 (m), 764.9 (m), 721.8 (vw)
Ce	3080 (ν_{OH}, w), 1618 (δ_{OH}, vw), 1478 (m), 1445 (w), 1431 (m), 1429 (m), 1259 (ν_{NO}, m), 1238 (ν_{NO}, s), 1230 (ν_{NO}, m), 1215 (ν_{NO}, s), 1160 (vw), 1121 (vw), 1106 (vw), 1035 (vw), 851.2 (m), 836.0 (m), 773.2 (m), 764.4 (m), 719.8 (vw)

Table S8 Raman data for **1Ln**

Lanthanide	Raman Shift (514 nm, cm^{-1})
Lu	3095 (m), 2199 ($\nu_{CN,}$ s), 1625 (m), 1608 (s), 1575 (m), 1512 (w), 1318 (s), 1264 (s), 1163 (w), 1052 (m), 864 (w), 739 (s), 640 (vw), 594 (vw), 558 (vw), 492 (vw), 452 (w), 299 (w), 283 (m), 162 (s), 125 (s)
Tb	3096 (m), 2199 (ν_{CN}, vs), 1625 (s), 1607 (m), 1575 (w), 1511 (vw), 1318 (s), 1264 (s), 1219 (w), 1161 (w), 1053 (m), 863 (w), 738 (m), 641 (vw), 592 (vw), 558 (vw), 489 (vw), 452 (m), 283 (w), 159 (m), 128 (s)
Eu*	2199 (ν_{CN}, vs), 1624 (s), 1607 (m), 1574 (w), 1511 (vw), 1317 (s), 1263 (s), 1219 (w), 1163 (w), 1052 (m), 862 (w), 737 (m), 640 (vw), 586 (vw), 558 (vw), 488 (vw), 452 (m), 282 (w), 148 (m), 129 (s)
Ce	3095 (m), 2199 (ν_{CN}, m), 1625 (m), 1606 (s), 1574 (w), 1511 (vw), 1317 (s), 1262 (s), 1219 (w), 1166 (w), 1126 (vw), 1053 (m), 1037 (w), 864 (w), 736 (s), 640 (vw), 592 (vw), 558 (vw), 489 (vw), 453 (vw), 281 (w), 152 (m), 127 (m)

*High frequency Raman peaks for **1Eu** obscured by Eu^{3+} photoluminescence ($^5D_0 \rightarrow {}^7F_J$ (J = 1,2) transitions appear at *ca*. 2650 and 3220 cm^{-1}, respectively, under 514 nm excitation).

Table S9 Elemental Analyses for **1Ln**

Lanthanide	Empirical Formula		C (%)	H (%)	N (%)
Lu	$C_{52}H_{34}N_{20}Au_3LuO_9$	Calcd:	33.78	1.85	15.15
		Found:	33.96	1.81	15.09
Tb	$C_{52}H_{34}N_{20}Au_3O_9Tb$	Calcd:	34.08	1.87	15.28
		Found:	34.09	1.87	14.82
Eu	$C_{52}H_{34}N_{20}Au_3EuO_9$	Calcd:	34.21	1.88	15.34
		Found:	34.42	1.86	15.35
Ce	$C_{52}H_{34}N_{20}Au_3CeO_9$	Calcd:	34.43	1.89	15.44
		Found:	34.42	1.88	15.02

Table S10 Crystallographic Data*

	1Lu	**1Tb**	**1Eu**	**1Ce**
Empirical formula	$C_{52}H_{34.66}Au_3LuN_{20}O_{9.33}$	$C_{52}H_{34.34}Au_3N_{20}O_{9.17}Tb$	$C_{52}H_{34.5}Au_3EuN_{20}O_{9.25}$	$C_{52}H_{34.4}Au_3CeN_{20}O_{9.2}$
F.W. (g mol^{-1})	1854.78	1835.89	1830.40	1817.59
Crystal System	Orthorhombic	Orthorhombic	Orthorhombic	Orthorhombic
Space Group	*Pbca*	*Pbca*	*Pbca*	*Pbca*
a (Å)	19.9815(12)	20.0668(9)	20.1041(11)	20.2203(7)
b (Å)	23.8662(12)	23.8472(1)	23.8591(14)	23.8559(8)
c (Å)	23.8919(13)	23.9197(8)	23.9360(14)	23.9799(9)
V (Å^3)	11,393.6(11)	11,446.5(8)	11,481.3(11)	11,567.3(7)
Z	8	8	8	8
T (K)	100(2)	100(2)	100(2)	100(2)
ρ_{calcd} (g cm^{-1})	2.163	2.131	2.118	2.087
μ (mm^{-1})	9.494	8.961	8.794	8.431
R_1, wR_2 $[I_0 \geq 2\sigma (I_0)]$	0.0468, 0.0745	0.0311, 0.0619	0.0355, 0.0769	0.0244, 0.0461
Goodness of fit	1.052	1.036	1.019	1.019

*Empirical formula and formula weight derived from the crystallographic model, thus, the water molecule O10 with partial occupancy is included.

Supplementary Figures

Figure S1: Shape of $[Lu(bipyO_2)_4]^{3+}$ cation in the structure of $[Lu(bipyO_2)_4](ClO_4)_3 \cdot 2H_2O$.[25] Orange circles represent ring centroids and π-π interactions are shown with dotted orange lines.

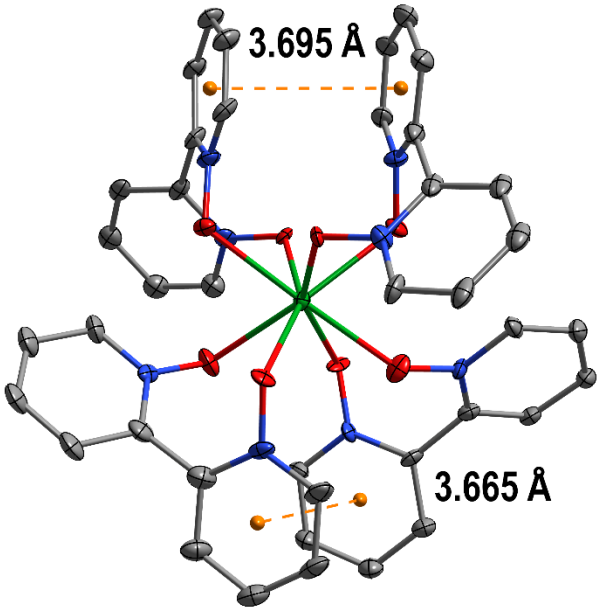

Figure S2: Comparison of $[Lu(bipyO_2)_4]^{3+}$ cation shapes in the structures of **1Lu** (blue) and $[Lu(bipyO_2)_4](ClO_4)_3 \cdot 2H_2O$ (red).[25]

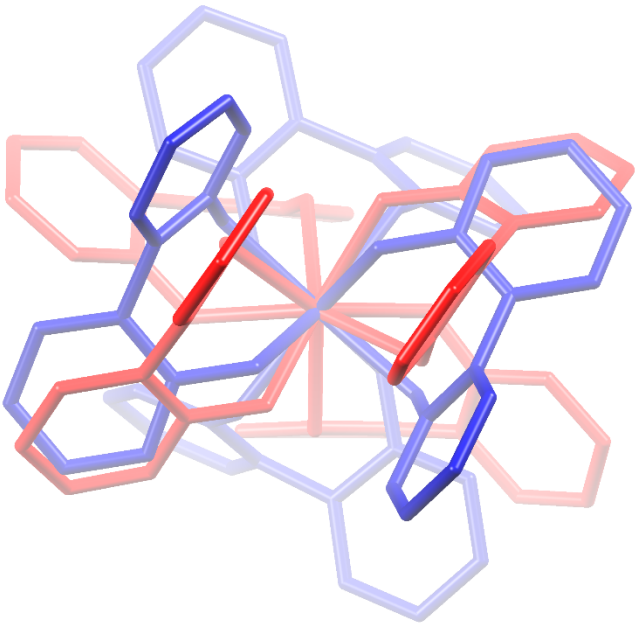

Figure S3: Continuous shape measures of selected $[Ln(bipyO_2)_4]^{3+}$ complexes plotted on the square antiprismatic-cubic shape map (See Table S3). For reference, the continuous shape measures of selected ideal polyhedra are plotted alongside: Cubic, square antiprismatic (SAP), and dodecahedral (Dod). The minimum distortion path between cubic and antiprismatic geometry is shown in red.

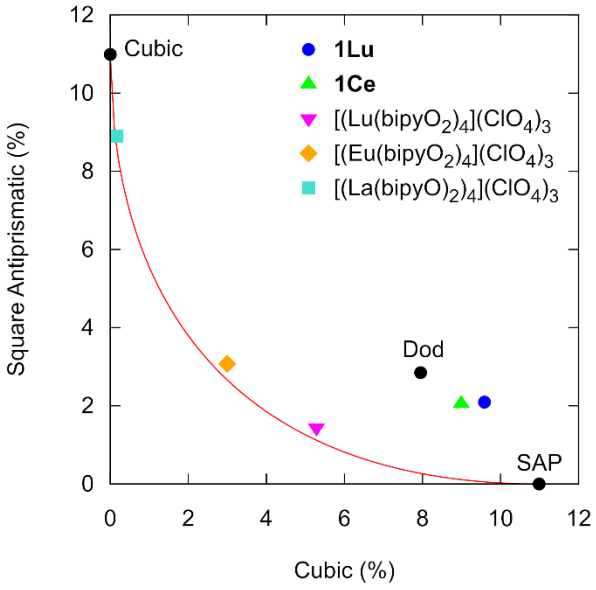

Figure S4: Non-covalent interactions around the $\{[Au(CN)_4]_3\}^{3-}$ trimer in the structure of **1Lu**. Au(III)···Au(III) interactions shown as yellow lines, Au···N interactions shown as light blue lines, and hydrogen bonds shown as dotted lines.

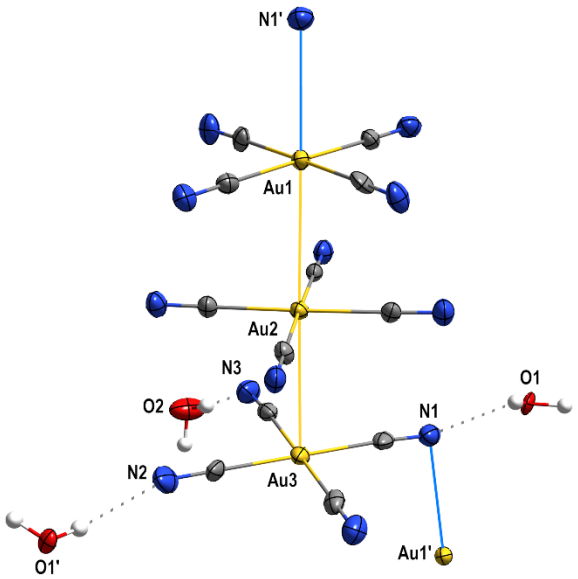

Figure S5: Au(III)···Au(III) distances in **1Ln** structures at 100 K plotted versus Shannon eight-coordinate trivalent lanthanide ionic radii.[27] Lines represent linear fits of the data. Error bars are within the points.

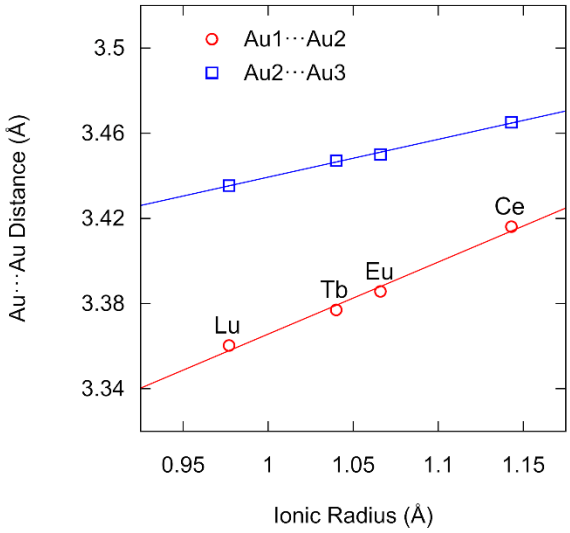

Figure S6: Calculated potential energy surface acquired by varying the Au···Au distance for a $\{[Au(CN)_2]\}^{2-}$ dimer (inset). A minimum is indicated at *ca.* 3.5 Å. The combined energy of the two $[Au(CN)_4]^-$ units is set to 0 kJ /mol at 4.4 Å

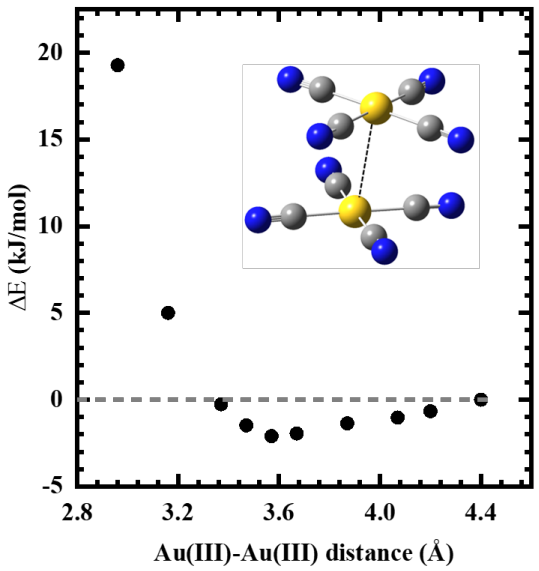

Figure S7: Normalized luminescence spectra for **1Lu** at 77 K. Excitation spectrum shown in blue, λ_{em} = 525 nm; emission spectrum shown in green, λ_{ex} = 310 nm. (*Erroneous peak from Eu^{3+} contamination in $LuCl_3 \cdot 6H_2O$ starting reagent, 99.9% trace metals basis).

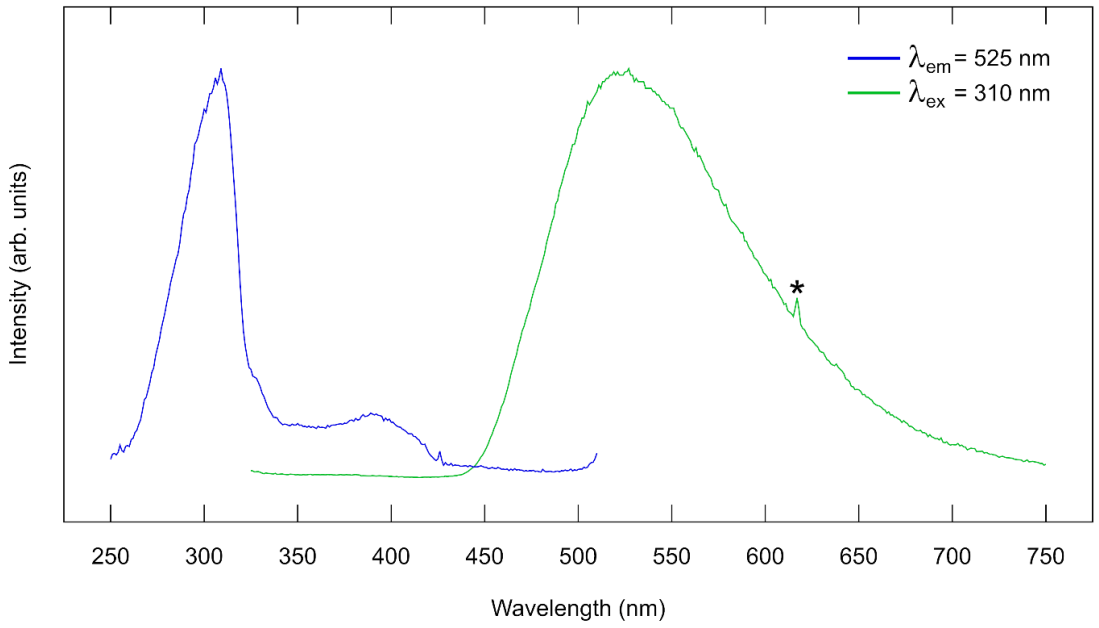

Figure S8: 2-D excitation/emission map for **1Lu** at 77 K.

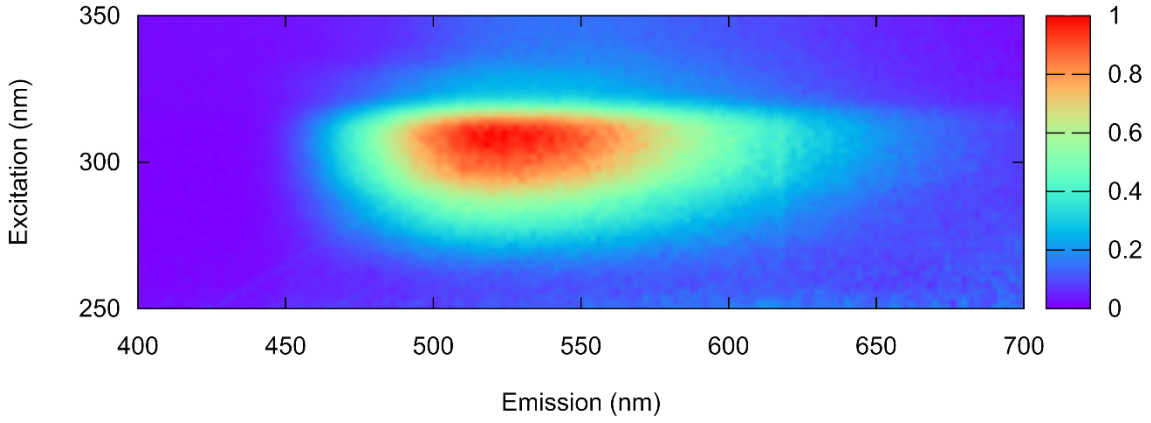

Figure S9: Normalized luminescence spectra for **1Tb** at 300 K (bottom spectra: excitation shown in blue, λ_{em} = 549 nm; emission shown in green, λ_{ex} = 340 nm) and 77 K (top spectra: excitation shown in light-blue, λ_{em} = 549.5 nm; emission shown in light-green, λ_{ex} = 340 nm).

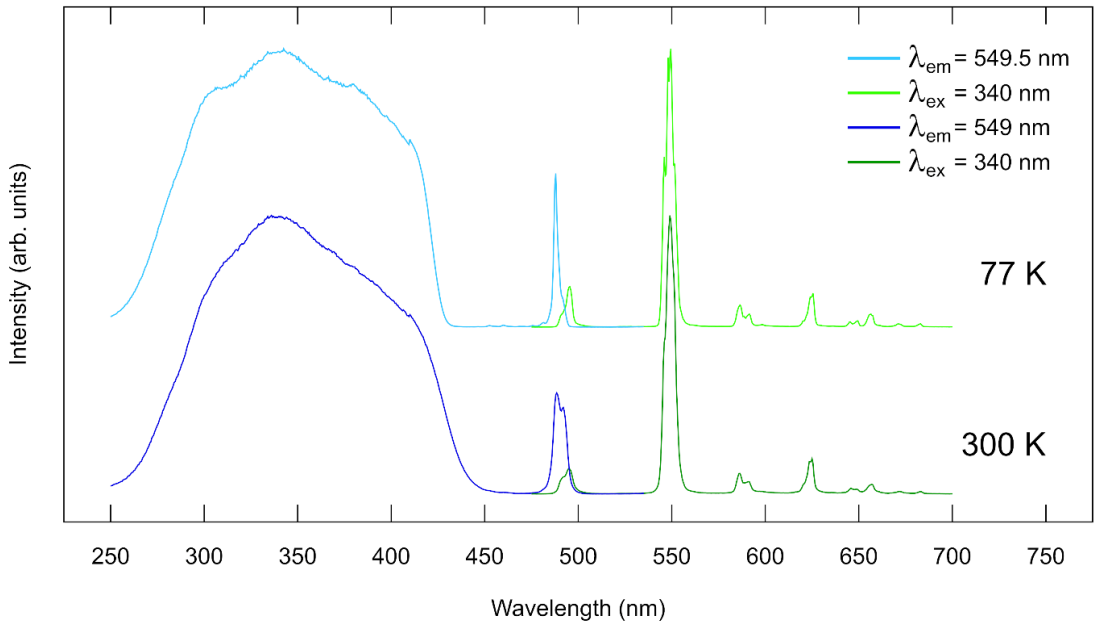

Figure S10: Commission internationale de l'éclairage (CIE) 1931 *xy* chromaticity diagram displaying the chromaticity coordinates for **1Tb** (0.329, 0.632) and **1Eu** (0.673, 0.323) calculated from their emission spectra. Wavelength values (nm) for the monochromatic locus shown in blue.

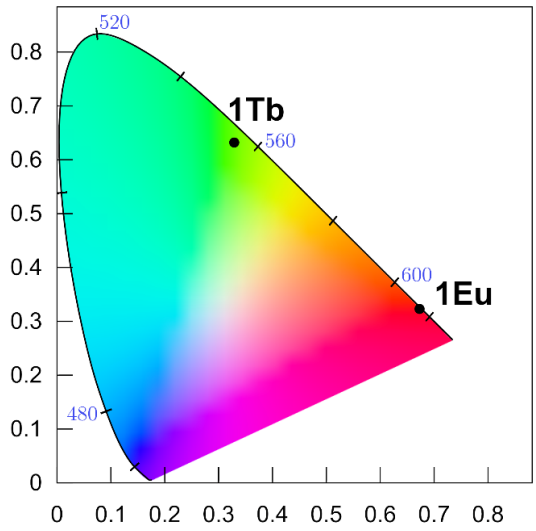

Figure S11: A photo of a single crystal of **1Ce**, displaying its large (cm-scale) size.

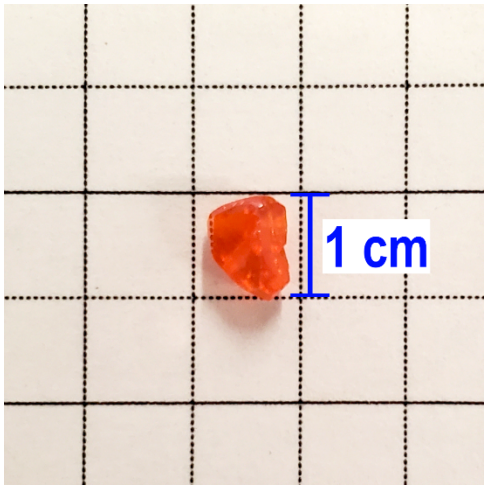

Figure S12: 300 K Powder X-Ray diffraction pattern for **1Eu** (red), compared to the pattern simulated from the single-crystal structure of **1Eu** at 300 K (blue) and 100 K (green).

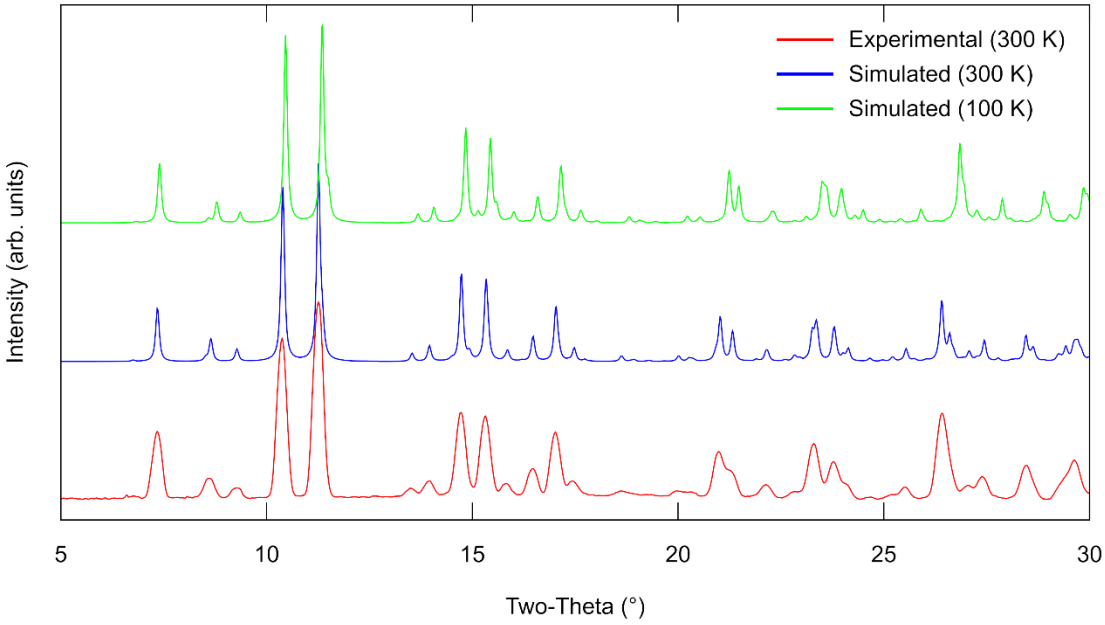

References

(1) Wrighton, M. S.; Ginley, D. S.; Morse, D. L. Technique for the Determination of Absolute Emission Quantum Yields of Powdered Samples. *J. Phys. Chem.* **1974**, *78* (22), 2229–2233. https://doi.org/10.1021/j100615a009.

(2) de Sá, G. F.; Malta, O. L.; de Mello Donegá, C.; Simas, A. M.; Longo, R. L.; Santa-Cruz, P. A.; da Silva, E. F. Spectroscopic Properties and Design of Highly Luminescent Lanthanide Coordination Complexes. *Coord. Chem. Rev.* **2000**, *196* (1), 165–195. https://doi.org/10.1016/S0010-8545(99)00054-5.

(3) Malta, O. L.; Legendziewicz, J.; Huskowska, E.; Turowska-Tyrk, I.; Albuquerque, R. Q.; de Mello Donegá, C.; e Silva, F. R. G. Experimental and Theoretical Study of Ligand Field, 4*f*–4*f* Intensities and Emission Quantum Yield in the Compound $Eu(bpyO_2)_4(ClO_4)_3$. *J. Alloys Compd.* **2001**, *323–324*, 654–660. https://doi.org/10.1016/S0925-8388(01)01027-1.

(4) Krause, L.; Herbst-Irmer, R.; Sheldrick, G. M.; Stalke, D. Comparison of Silver and Molybdenum Microfocus X-Ray Sources for Single-Crystal Structure Determination. *J. Appl. Crystallogr.* **2015**, *48* (1), 3–10. https://doi.org/10.1107/S1600576714022985.

(5) Sheldrick, G. M. SHELXT – Integrated Space-Group and Crystal-Structure Determination. *Acta Crystallogr. Sect. A* **2015**, *71* (1), 3–8. https://doi.org/10.1107/S2053273314026370.

(6) Dolomanov, O. V.; Bourhis, L. J.; Gildea, R. J.; Howard, J. a. K.; Puschmann, H. OLEX2: A Complete Structure Solution, Refinement and Analysis Program. *J. Appl. Crystallogr.* **2009**, *42* (2), 339–341. https://doi.org/10.1107/S0021889808042726.

(7) Sheldrick, G. M. Crystal Structure Refinement with SHELXL. *Acta Crystallogr. Sect. C* **2015**, *71* (1), 3–8. https://doi.org/10.1107/S2053229614024218.

(8) Momma, K.; Izumi, F. *VESTA*: A Three-Dimensional Visualization System for Electronic and Structural Analysis. *J. Appl. Crystallogr.* **2008**, *41* (3), 653–658. https://doi.org/10.1107/S0021889808012016.

(9) Macrae, C. F.; Sovago, I.; Cottrell, S. J.; Galek, P. T. A.; McCabe, P.; Pidcock, E.; Platings, M.; Shields, G. P.; Stevens, J. S.; Towler, M.; Wood, P. A. Mercury 4.0: From Visualization to Analysis, Design and Prediction. *J. Appl. Crystallogr.* **2020**, *53* (1), 226–235. https://doi.org/10.1107/S1600576719014092.

(10) Sevvana, M.; Ruf, M.; Usón, I.; Sheldrick, G. M.; Herbst-Irmer, R. Non-Merohedral Twinning: From Minerals to Proteins. *Acta Crystallogr. Sect. F* **2019**, *75* (12), 1040–1050. https://doi.org/10.1107/S2059798319010179.

(11) Frisch, M. J. et al. Gaussian 16. **2016**.

(12) Mendizabal, F.; Pyykkö, P. Aurophilic Attraction in Binuclear Complexes with Au(I) and Au(III). A Theoretical Study. *Phys. Chem. Chem. Phys.* **2004**, *6* (5), 900–905. https://doi.org/10.1039/B313666C.

(13) Blasco, D.; Reboiro, F.; Sundholm, D.; Olmos, M. E.; Monge, M.; López-de-Luzuriaga, J. M. A "Gold Standard" Computational Proof for the Existence of Gold(III) Aurophilicity. *Dalton Trans.* **2023**, *52* (8), 2219–2222. https://doi.org/10.1039/D2DT03731A.

(14) Lara, D.; Santibañez, D.; Miranda-Rojas, S.; Mendizabal, F. Is There a Covalent Au(I)–Au(I) Bond in the Trans-$(AuX)_2$ (X = F, Cl, Br, I) Structure? A Post-Hartree–Fock and Density Functional Theory Study. *Inorg. Chem.* **2023**, *62* (38), 15421–15431. https://doi.org/10.1021/acs.inorgchem.3c01547.

(15) Reiher, M. Douglas–Kroll–Hess Theory: A Relativistic Electrons-Only Theory for Chemistry. *Theor. Chem. Acc.* **2006**, *116* (1), 241–252. https://doi.org/10.1007/s00214-005-0003-2.
(16) Cirera, J.; Ruiz, E.; Alvarez, S. Shape and Spin State in Four-Coordinate Transition-Metal Complexes: The Case of the D6 Configuration. *Chem. – Eur. J.* **2006**, *12* (11), 3162–3167. https://doi.org/10.1002/chem.200501516.
(17) Casanova, D.; Llunell, M.; Alemany, P.; Alvarez, S. The Rich Stereochemistry of Eight-Vertex Polyhedra: A Continuous Shape Measures Study. *Chem. – Eur. J.* **2005**, *11* (5), 1479–1494. https://doi.org/10.1002/chem.200400799.
(18) Pinsky, M.; Avnir, D. Continuous Symmetry Measures. 5. The Classical Polyhedra. *Inorg. Chem.* **1998**, *37* (21), 5575–5582. https://doi.org/10.1021/ic9804925.
(19) Chernyshev, A. N.; Chernysheva, M. V.; Hirva, P.; Kukushkin, V. Yu.; Haukka, M. Weak Aurophilic Interactions in a Series of Au(III) Double Salts. *Dalton Trans.* **2015**, *44* (32), 14523–14531. https://doi.org/10.1039/C4DT03167A.
(20) Bardina, E. E.; Makotchenko, E. V.; Birin, K. P.; Baidina, I. A.; Sukhikh, T. S.; Novikov, A. S.; Gorbunova, Y. G.; Tsivadze, A. Y.; Gushchin, A. L. Noncovalent Interactions in Gold(III) Tetrakis(4-Butoxyphenyl)Porphyrinate Structures. *CrystEngComm* **2023**, *25* (33), 4755–4767. https://doi.org/10.1039/D3CE00428G.
(21) Au, V. K.-M.; Lam, W. H.; Wong, W.-T.; Yam, V. W.-W. Luminescent Cyclometalated Alkynylgold(III) Complexes with 6-Phenyl-2,2′-Bipyridine Derivatives: Synthesis, Characterization, Electrochemistry, Photophysics, and Computational Studies. *Inorg. Chem.* **2012**, *51* (14), 7537–7545. https://doi.org/10.1021/ic300140w.
(22) Hayoun, R.; Zhong, D. K.; Rheingold, A. L.; Doerrer, L. H. Gold(III) and Platinum(II) Polypyridyl Double Salts and a General Metathesis Route to Metallophilic Interactions. *Inorg. Chem.* **2006**, *45* (16), 6120–6122. https://doi.org/10.1021/ic060830z.
(23) Klapötke, T. M.; Krumm, B.; Galvez-Ruiz, J.-C.; Nöth, H. Highly Sensitive Ammonium Tetraazidoaurates(III). *Inorg. Chem.* **2005**, *44* (26), 9625–9627. https://doi.org/10.1021/ic051543i.
(24) Lu, W.; Chan, K. T.; Wu, S.-X.; Chen, Y.; Che, C.-M. Quest for an Intermolecular Au(III)···Au(III) Interaction between Cyclometalated Gold(III) Cations. *Chem. Sci.* **2012**, *3* (3), 752–755. https://doi.org/10.1039/C2SC00947A.
(25) Huskowska, E.; Turowska-Tyrk, I.; Legendziewicz, J.; P. Riehl, J. The Structure and Spectroscopy of Lanthanide(III) Complexes with 2,2′-Bipyridine-1,1′-Dioxide in Solution and in the Solid State: Effects of Ionic Size and Solvent on Photophysics, Ligand Structure and Coordination. *New J. Chem.* **2002**, *26* (10), 1461–1467. https://doi.org/10.1039/B201846M.
(26) Al-Karaghouli, A. R.; Day, R. O.; Wood, J. S. Crystal Structure of Tetrakis(2,2'-Bipyridine Dioxide)Lanthanum Perchlorate: An Example of Cubic Eight-Coordination. *Inorg. Chem.* **1978**, *17* (12), 3702–3706. https://doi.org/10.1021/ic50190a076.
(27) Shannon, R. D. Revised Effective Ionic Radii and Systematic Studies of Interatomic Distances in Halides and Chalcogenides. *Acta Crystallogr. Sect. A* **1976**, *32* (5), 751–767. https://doi.org/10.1107/S0567739476001551.